Physical and Electroresponsive Characteristics of the Intercalated Styrene-Acrylonitrile Copolymer/Clay Nanocomposite under Applied Electric Fields

J. W. Kim,[1] L. W. Jang,[1] H. J. Choi,[1] M. S. Jhon[2]

[1]*Department of Polymer Science and Engineering, Inha University, Incheon, 402-751, Korea*
[2]*Department of Chemical Engineering, Carnegie Mellon University, Pittsburgh, Pennsylvania 15213*

Received 19 July 2002; accepted 25 October 2002

ABSTRACT: Styrene-acrylonitrile copolymer (SAN)/clay nanocomposites were synthesized through an emulsion copolymerization of styrene and acrylonitrile in the presence of sodium montmorillonite, and their physical properties and electroresponsiveness under an applied electric field were characterized. Thermogravimetric analysis (TGA) showed that the thermal stability of the synthesized polymer was sustained. X-ray diffraction (XRD) analysis confirmed the insertion of SAN into the interlayers of clay, whose separation consequently increased, as compared to those of the pristine clay. Transmission electron microscopy (TEM) was used to observe the suspended state of clay. Dry-base electrorheological (ER) fluids were prepared by mixing intercalated SAN nanocomposite particles into silicone oil. Typical ER behavior, i.e., enhancement of shear and yield stresses in the presence of an applied electric field, was observed using a rotational rheometer equipped with a high-voltage generator. A universal yield stress scaling equation was also found to fit our experimental data well.
 J Appl Polym Sci 89: 821–827, 2003

Key words: electrorheological fluid; SAN copolymer; emulsion polymerization; nanocomposite

INTRODUCTION

Because they use molecular or nanoscale reinforcement techniques instead of conventional particulate-filled composites, polymer nanocomposites have recently attracted considerable attention due to their enhanced properties and ability to extend their utility, by which they offer unique characteristics that are drastically different from their bulk counterparts.[1] These characteristics include increased moduli, strength, and barrier characteristics, and high distortion temperature and electrical conductivity.[2–9] Various nanocomposites have been synthesized by different preparation methods, including polymer intercalation into the layers of clay, in which clay minerals are introduced because of their small particle size and layer expanding capabilities, especially in the development of reinforcement materials.[10,11]

A large number of polymer/clay nanocomposites have become accessible in the form of end-functionalized derivatives,[12,13] and montmorillonite (MMT) has been widely used to syntheses the nanocomposite.[14] Layered smectite-type MMT, a hydrous alumina silicate mineral whose lamellae are constructed from octahedral alumina sheets sandwiched between two tetrahedral silicate sheets, exhibits a net negative charge on the lamellar surface, which adsorbs cations such as Na^+ or Ca^{++}. Compatibility with various polymers is accomplished by modifying the silicates with alkylammonium cations via an ion exchange reaction.[14]

When the clay is exchanged with Na^+ it possesses an excellent swelling rate in water, and its interlayer spacing becomes large enough for monomer penetration. Using this concept, emulsion intercalations for polyaniline (PANI),[15,16] polystyrene (PS),[17] ethylene-vinyl acetate copolymer,[18] and styrene-acrylonitrile copolymer (SAN)[19] with Na^+-MMT nanocomposites have been introduced. The emulsion polymerization has the advantage of being able to simultaneously attain both high molecular weights and high reaction rates.

The electrorheological (ER) fluid characteristics of synthesized polymer/clay nanocomposite suspended in silicone oil were recently reported.[15]

ER fluids are heterogeneous colloidal suspensions whose properties strongly depend on an applied electric field in which a characteristic fibrillation with the strings of particles oriented along the direction of an electric field is observed. This fibrillation of particles is due to the electric field production of a significant increase in apparent viscosity,[20] and due to their emerging technological applications,[21,22] ER fluids have been the subject of intense theoretical and experimental research.

Correspondence to: H. J. Choi (hjchoi@inha.ac.kr).

Most electroresponsive particles, especially those in hydrous systems, are known to require the addition of small quantities of water or other polar additives such as surfactant to produce ER behavior. Various wet-base ER materials including corn starch,[23] silica gel,[24] mesoporous molecular sieve,[25] and cellulose[26] have been investigated. In wet-base systems with hydrophilic particles, the particle chain structure develops when ions migrate in the absorbed water. However, hydrous ER fluids have disadvantages in engineering applications due to the presence of water. Therefore, various anhydrous ER fluids, including semiconducting polymer particles, have been developed to overcome these obstacles. These anhydrous ER materials, which have the advantage of a broad working temperature range, possess reduced device abrasion and a relatively low current density. In addition, they have intrinsic charge carriers in either the bulk particles or their surfaces that can move locally under an applied electric field. Examples include dehydrated zeolite,[27,28] rare-earth-doped TiO_2,[29] and several semiconducting polymers, such as PANI,[30,31] copolyaniline,[32] poly(acene quinone) radicals,[33] polyphenylenediamine,[34] microencapsulated PANI,[35] phosphate cellulose,[36] and polymer/clay nanocomposites.[37] Recently, PANI/Na^+-MMT,[37] polypyrrole/clay,[38] and SAN/clay nanocomposite particles[39] synthesized by emulsion polymerization were used as ER materials.

In this study, we synthesized the SAN/Na^+-MMT nanocomposite particles via an emulsion polymerization. We characterized their physical properties via Fourier transform-infrared (FT-IR) spectroscopy, X-ray diffraction (XRD), thermogravimetric analysis (TGA), gel permeation chromatography (GPC), and transmission electron microscope (TEM). This direct and one-step polymerization produces SAN-intercalted nanocomposites without significant exfoliation. We then prepared ER suspensions using these particles and observed their ER characteristics. We employed a generalized scaling function, which is a convenient form analyzing ER data.

EXPERIMENTAL

Synthesis of the SAN/clay nanocomposite

For an emulsion polymerization of polymer nanocomposites, Na^+-MMT clay (supplied from Southern Clay Product) was adopted to synthesize a polymer/clay nanocomposite with SAN in the presence of potassium persulfate and sodium lauryl sulfate (SDS). Initially, a 2 l four-neck flask was charged with 600 ml of aqueous dispersions containing the proper amount of Na^+-MMT. After the clay solution was sonicated for 1 hr at 60°C using a custom-made ultrasonicator with 750 W of 28 kHz sound,[40] styrene/acrylonitrile monomers (70/30 wt %), SDS, and potassium persulfate ($K_2S_2O_8$) were added during agitation. The copolymerization was initiated by raising the temperature to 82°C, and the emulsion polymerization was continued for 8 h with a stirring rate of 450 rpm. The coagulated products were subjected to a series of intensive washings via four cycles of centrifugation and redispersion into water. The reaction was terminated by adding 700 m*l* of aluminum sulfate solution (10 wt %). The products were then vacuum dried at 60°C for two days. The final weight fraction of the Na^+-MMT in the SAN/clay nanocomposite was 4.76 wt %.

TABLE I
Sample Code of Various SAN/Clay Nanocomposites Used in This Study

Sample code	SAN/Clay	Extraction	Ratio of particle to liquid oil for ER fluid (wt %)
SANU5	5/100	x	—
SANE5	5/100	o	—
SAER10	5/100	x	10
SAER20	5/100	x	20
SAER25	5/100	x	25

Characterization of the SAN/clay nanocomposite

Chemical structures of the Na^+-MMT clay and synthesized SAN/Clay nanocomposite were examined by FT-IR analysis (Nicolet Spectrophotometer). Thermal characterizations were performed by both differential scanning calorimetry (DSC, Perkin-Elmer DSC 7, USA) and TGA (DuPont 9900, USA). The DSC measurements were carried out by heating 10 mg of the sample to 160°C at a heating rate of 10°C/min in a nitrogen atmosphere. TGA measurements were carried out by heating 20 mg of sample up to 700°C at a heating rate of 20°C/min in a nitrogen atmosphere. For an XRD analysis, a Guinier focusing camera using a quartz crystal monochromator in a Philips PW-1847 X-ray crystallographic unit fitted with a copper target was used (40 kV and 20 mA) for recording data in the range of $2\theta = 2 \sim 16°$. The average molecular weight of the polymers being recovered from the nanocomposite extracts were measured by Waters Model 201 equipped with a U6K injector, M6000A solvent delivery system, and three linear columns packed with μ-styragel. The phase morphology was examined by the TEM (Jeol-200 CX TEM) with an acceleration voltage of 200 kV image taken from the broken surface of a purified nanocomposite.

Characterization of the SAN/clay nanocomposite based ER suspension

Three different weight fractions (10, 20, and 25 wt %) of ER fluids with the synthesized SAN/clay nanocom-

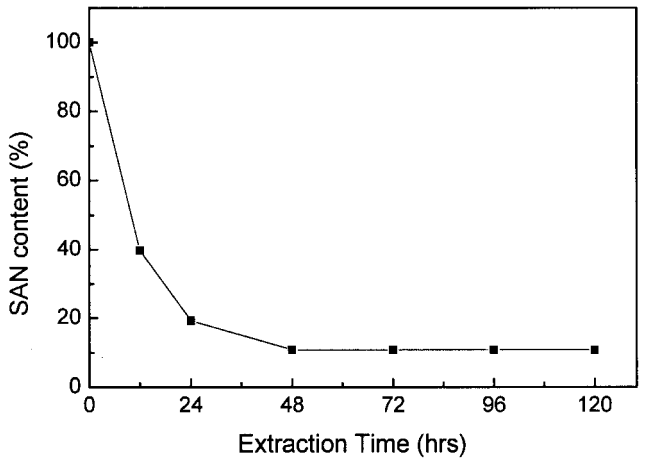

Figure 1 SAN content in SANU5 vs. extraction time

posite particle without extraction (SANU5) suspended silicone oil (viscosity of 30 cSt) were prepared. We called them as SAER10, SAER20 and SAER25, respectively. The suspensions were dispersed via a mechanical stirrer with rotational speed of 1,800 rpm. Rheological measurements were then carried out using a rotational rheometer (Physica MC120, Stuttgart, Germany) with a Couette geometry (Z3-DIN or Z4-DIN), a high voltage generator (HVG 5000), and an oil bath for temperature control. The gap sizes of the Z3-DIN and the Z4-DIN were 1.06 mm and 0.59 mm, and the maximum attainable stresses were 1.141 kPa and 6.501 kPa, respectively. The HVG 5000 can supply a DC voltage up to 10 kV within. The suspensions were placed in the gap between the stationary outer measuring cup and the rotating bob. An electric field was applied for few minutes to obtain a chainlike (or columnar) structure before applying shear. The shear rate varied from 10^{-1} to 10^{3} s^{-1}. The stress at the transition point where viscosity abruptly changed was interpreted by the yield stress. To measure the conductivity (two-probe method) of the SAN/clay nanocomposite material, pellets of dried composite particle were prepared, and the resistance of the pellet was measured by a picoammeter (Keithely 487).

RESULTS AND DISCUSSION

In order to measure not only the molecular weight of the synthesized SAN but also the amount of purely intercalated SAN in the interlayers of the clay, purification of the SAN/clay nanocomposite was accomplished by hot tetrahydrofuran (THF) extraction for five days. The molecular weight of SAN was determined by GPC using THF as a solvent. The weight-average molecular weight of the extracted SAN was 53,000 g/mol. Based on the limiting plateau of polymer loading after 48 h of extraction, as illustrated in Figure 1, it is clear that considerable amounts of copolymer remained even after five days of extraction. These residual unextractable polymers can be regarded as the copolymer intercalated in the MMT gallery.[41]

The copolymer in the composite, either extracted (SANE5) or unextracted (SANU5), is measured from TGA thermograms, as shown in Figure 2. In contrast to pure SAN, the onset of decomposition for the nanocomposites of either extracted or nonextracted copolymer was shifted towards a higher temperature, indicating an enhancement of the thermal stability upon intercalation.[42] In the case of the PS/MMT nanocomposite, Chen et al.[43] suggested that the higher decomposition onset temperature of a PS/MMT nanocomposite, as compared to that of PS, can be attributed to the MMT layers, which prevent diffusion of the volatile decomposition products.

DSC traces of the extracted and nonextracted nanocomposites and the SAN copolymer are shown in Figure 3. The copolymer containing about 19 wt % of acrylonitryl exhibits an endotherm at approximately 107°C (T_g), and those composites demonstrate an increasing trend of their T_g's with increasing amounts of MMT added. The appearance of T_g's, from those unpurified products is due mainly to the copolymers adsorbed on the outer surfaces of MMT, and the increasing trend of T_g is a consequence of the increased thermal insulation effect of MMT. Meanwhile, the DSC thermogram of extracted composites (SANE5) does not indicate any trace of a clear thermal transition due to the absence of a discrete polymer phase. This can be attributed to the fact that the confined polymer chains in the galley on the MMT are not free from chain motion, as is the case for the pristine copolymers.

XRD analysis shows that the interlayer spacing of the clay increases with an intercalation of SAN copol-

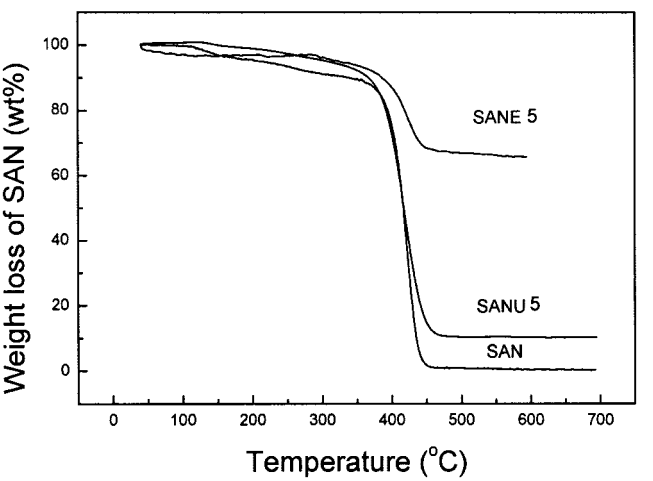

Figure 2 TGA thermograms of pure SAN copolymer (SAN), unextracted (SANU5), and extracted (SANE5) SAN-clay nanocomposites.

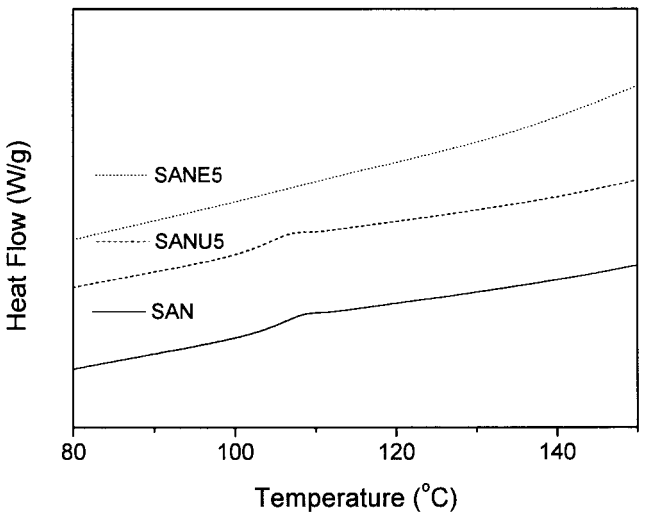

Figure 3 DSC thermograms of the SAN copolymer, unextracted (SANU5) and extracted (SANE5) SAN-clay nanocomposites.

ymer loading, as shown in Figure 4. The interlayer spacing increases from the base distance of the clay itself (11.1Å), with 2θ =7.5°, to that of the SAN/clay nanocomposites (17.4 Å) due to the insertion of the SAN copolymer. Furthermore, the intensive reflections of the composites compared to that of pristine MMT at 2θ = 5° indicate that the system is composed of alternating polymer and MMT layers. Accordingly, XRD analysis indicates that the SAN copolymer can also be intercalated in the interlayer of Na^+-MMT by the emulsion technique without accompanying significant delamination.[19]

Furthermore, in order to confirm the nanocomposite structures, the dispersibility of the silicate layers in the

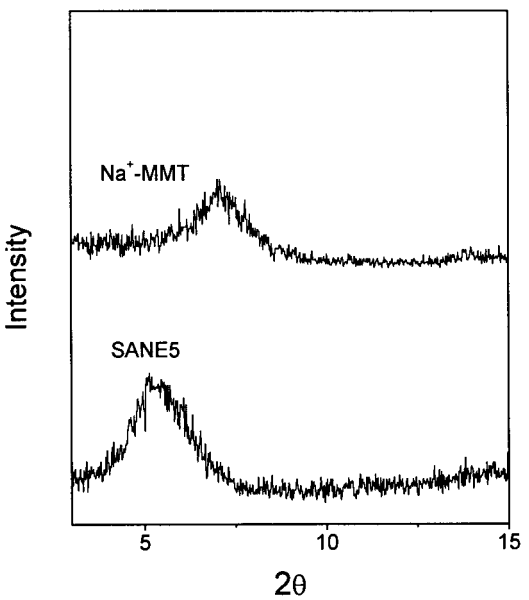

Figure 4 XRD patterns of the SANE5 and Na^+-MMT clay.

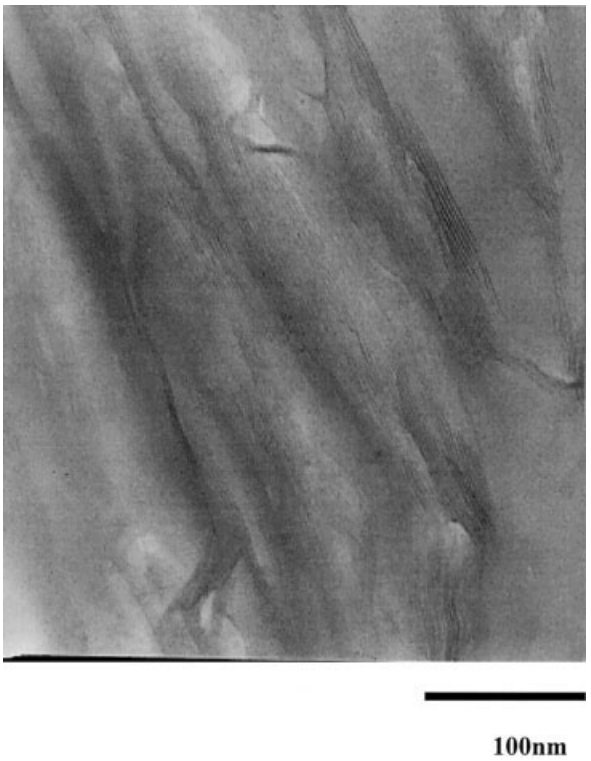

Figure 5 TEM image of unextracted SAN/clay nanocomposite (SANU5). Dark areas are the intercalated clay layers and bright areas are the SAN matrix.

SAER without extraction was observed via TEM. Clearly, Figure 5 shows that the 1–2 nm sized silicate layers are in a well ordered-state and have dispersed homogeneously in the copolymer matrix, thus confirming the formation of the intercalated nanocomposite. This result coincides with the enlargement of 001 spacing in the XRD analyses. Concurrently, this homogeneous dispersion suggests that exfoliation did not take place during the intercalation reaction process.

Figure 6 shows the flow curves obtained from the controlled shear rate mode test for 20 wt % suspensions of the SAN/clay composite with three different applied electric field strengths. The shear stress increases monotonically (but nonlinearly) with the shear rate in the absence of an applied electric field. Similar to most ER fluids, the SAN/clay-nanocomposite-based ER fluids show increased shear stresses. Figure 6 shows that the shear stress slightly decreases, following the plateau values of shear stress, then increases again as the shear rate increases. At lower shear rates, the fibrillated structure begins to be deformed, but the structure reforms immediately after the cessation of shear. At intermediate shear rates, the chain structures slowly break down. For higher shear rates, the fluid motion becomes more rapid and destroys the chain structure. In other words, as the destruction rate of the column structures becomes faster

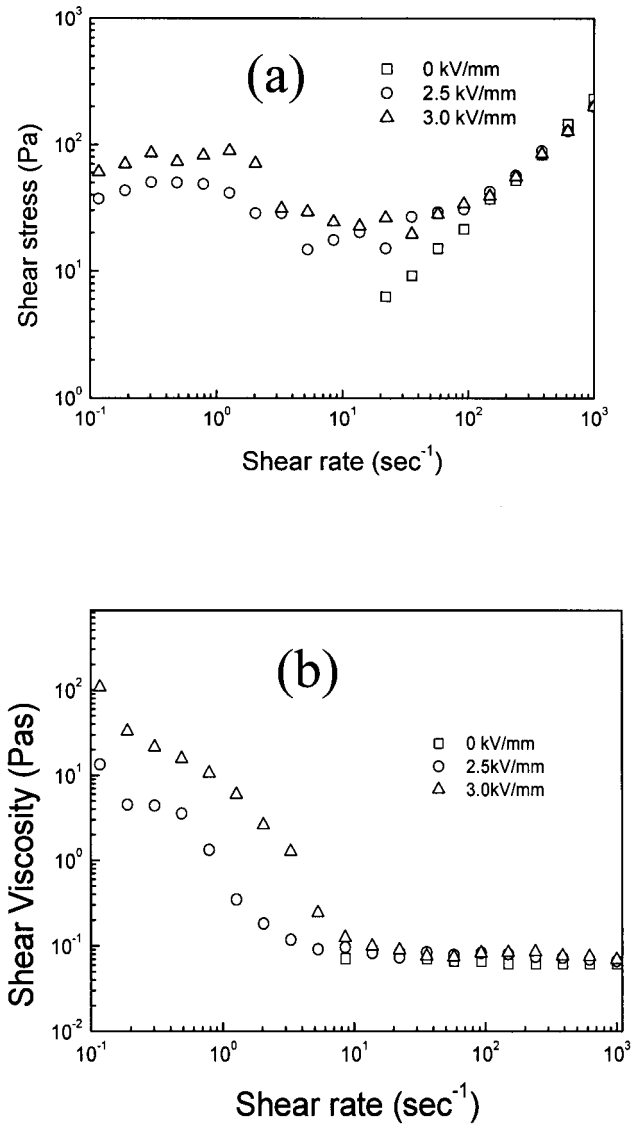

Figure 6 Flow curves for the SANU5-based ER suspensions with 20 wt % particle concentration (SAER20).

than the column reforming rate by the electric field, the flow curves behave much like those without an electric field. The fibril structures are then broken into particles or particle clusters by shearing due to dominant hydrodynamic interactions, and eventually the ER effect virtually disappears.

Several models have been proposed to describe shear stress in ER fluids equations.[44] The polarization model attributes the attractive force between particles to Maxwell–Wagner's interfacial polarization, representing that the yield stress $\tau_y \propto \phi K_f E_0^2 f(\beta)$, where ϕ is the volume fraction of the particles, E_0 is the applied electric field strength, and $(\beta = (K_p - K_f)/(K_p + 2K_f)$ is the dimensionless dielectric mismatch parameter. Here, K_p and K_f are the dielectric permittivities of the particle and the fluid, respectively. This polarization model shows excellent agreement with data for small values of ϕ and E_0.[45] However, yield stress significantly deviates from the polarization model at high electric field strengths and is better represented by the following power law: $\tau_y \propto E_0^m$ $(m \leq 2)$. As the gap between the conducting particles in the fluid decreases, the fluid's electric response becomes nonlinear due to electrical breakdown (or partial discharge) under the high electric field strengths. This nonlinear conductivity effect with the bulk conducting particle model was taken into account and a power law index m approaches 3/2 at high electric field strengths. Based on the nonlinear conductivity model[46] for ER fluids, good qualitative agreement exists between predicted and measured ER behavior for various ER systems.[47,48] Figure 7 shows that the power law indices decrease with particle concentration.

To represent the yield stress data for a broad electric field strength range, the following hybrid equation has been introduced:[49,50]

$$\tau_y(E_0) = \alpha E_0^2 \left(\frac{\tanh \sqrt{E_0/E_c}}{\sqrt{E_0/E_c}} \right), \tag{1}$$

where α depends on the dielectric constant of the fluid, and the particle volume fraction. E_c represents the critical electric field originating from the nonlinear conductivity model, and describes crossover behavior between the two regimes in the E_0 versus the τ_y plot. Eq. (1) has the following two limiting behaviors at low and high electric field strengths, respectively:

$$\tau_y = \alpha E_0^2 \propto E_0^2 \quad E_0 \ll E_c \tag{2a}$$

$$\tau_y = \alpha \sqrt{E_c} E_0^{3/2} \propto E_0^{3/2} \quad E_0 \gg E_c \tag{2b}$$

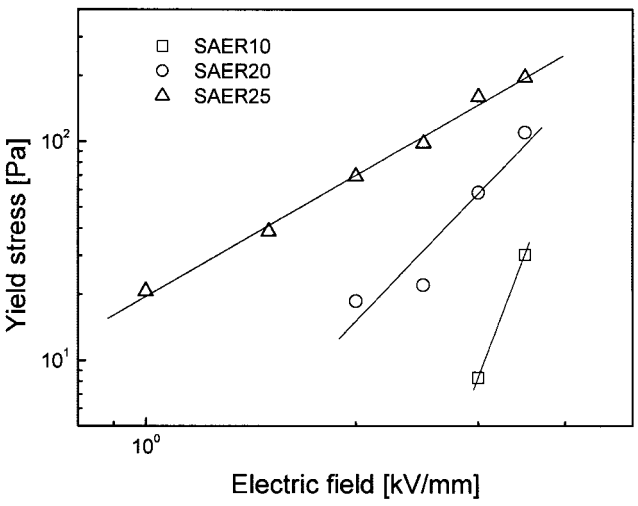

Figure 7 Yield stress vs. applied electric field for three different particle concentrations of SAER series.

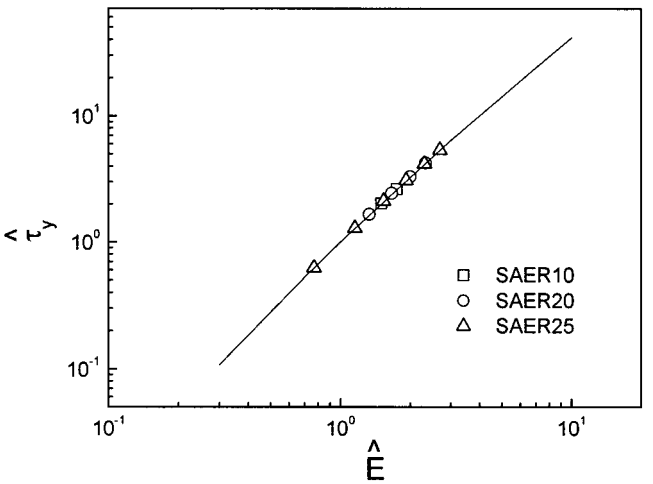

Figure 8 $\hat{\tau}$ vs. $\hat{E}$ (scaled function) for SAER10, SAER20 and SAER25.

Eq. (2a) shows that τ_y is proportional to E_0^2 at a low E_0, and τ_y changes abruptly to$E_0^{3/2}$, transferring to another regime at a high E_0. In a previous investigation with various ER fluids' data,[50] we found that E_c is affected by the conductivity mismatch between the particle and medium liquid, and is weakly dependent on the volume fraction. To collapse our data into a single curve, we normalized eq. (1) with E_c and $\tau_y(E_c) = 0.762\alpha E_c^2$:

$$\hat{\tau} = 1.313\hat{E}^{3/2} \tanh \sqrt{\hat{E}}, \qquad (3)$$

where $\hat{E} \equiv E_0/E_c$ and $\hat{\tau} \equiv \tau_y(E_0)/\tau_y(E_c)$. By using eq. (3), the yield stress data for the SAN/clay-nanocomposite-based ER fluids collapse onto a single curve and are independent of particle concentration, as shown in Figure 8.

CONCLUSIONS

The SAN copolymer intercalated MMT nanocomposites were prepared by emulsion intercalation. The XRD patterns for the composite purified by hot extraction show 001 basal spacing enlargement by as much as 1.60 nm, without accompanying exfoliation of clay. Thermal characterization by TGA for those purified composites provides evidence of an enhanced onset temperature of thermal decomposition, however, the DSC thermogram did not exhibit any trace of thermal transition, due to the restricted molecular motion of confined polymer chains. TEM measurements for unpurified samples reveal homogeneous dispersion of a 1–2 nm sized silicate layer in the copolymer matrix. The intercalated particles were used for ER fluid, showing typical ER behavior such that both yield stress and enhanced shear stress of the ER suspension were observed as functions of applied electric field and shear rate. Furthermore, the yield stresses of the SAERs were found to fit with a universal scaling curve.

This work was supported by research grants from the Korea Science and Engineering Foundation (KOSEF) through the Applied Rheology Center (ARC), an official KOSEF-created engineering research center (ERC) at Korea University, Korea.

References

1. Caseri, W. Macromol. Rapid Commun. 2000, 21, 705.
2. Leroux, F.; Besse, J.P. Chem Mater 2001, 13, 3507.
3. Reichert, P.; Hoffmann, B.; Bock, T.; Thomann, R.; Mülhaupt, R.; Friedrich, C. Macromol Rapid Commun 2001, 22, 519.
4. Ryu, J.G.; Lee, P.S.; Kim, H.; Lee, J.W. Korea-Australia Rheol. J 2001, 13, 61.
5. Wu, Q.J.; Liu, X.H.; Berglund, L.A. Macromol Rapid Commun 2001, 22, 1438.
6. Lim, S.T.; Hyun, Y.H.; Choi, H.J.; Jhon, M.S. Chem Mater 2002, 14, 1839.
7. Alexandre, M.; Beyer, G.; Henrist, C.; Cloots, R.; Rulmant, A.; Jerome, R.; Dubois, P. Macromol Rapid Commun 2001, 22, 643.
8. Hyun, Y.H.; Lim, S.T.; Choi, H.J.; Jhon, M.S. Macromolecules 2001, 34, 8084.
9. Fong, H.; Vaia, R.A.; Sanders, J.H.; Lincoln, D.; Vreugdenhil, A.J.; Liu, W.D.; Bultman, J.; Chen, C.G. Chem Mater 2001, 13, 4123.
10. Tjong, S.C.; Meng, Y.Z.; Hay, A.S. Chem Mater 2002, 14, 44.
11. Manias, E.; Touny, A.; Wu, L.; Strawhecker, K.; Lu, B. Chung, T.C. Chem Mater 2001, 13, 3516.
12. Jin, Y.H.; Park, H.J.; Im, S.S.; Kwak, S.Y.; Kwak, S. Macromol Rapid Commun 2002, 23, 135.
13. Wang, H.S.; Zhao, T.; Zhi, L.J.; Yan, Y.H.; Yu, Y.Z. Macromol Rapid Commun 2002, 23, 44.
14. Alexandre, M.; Dubois, P. Mater Sci Eng Rev 2000, 28, 1.
15. Kim, J.W.; Kim, S.G.; Choi, H.J.; Jhon, M.S. Macromol Rapid Commun 1999, 20, 450.
16. Kim, B.H.; Jung, J.H.; Joo, J.; Epstein, A.J.; Mizoguchi, K.; Kim, J.W.; Choi, H.J. Macromolecules 2002, 35, 1419.
17. Kim, T.H.; Jang, L.W.; Lee, D.C.; Choi, H.J.; Jhon, M.S. Macromol. Rapid Commun. 2002, 23, 191.
18. Alexandre, M.; Beyer, G.; Henrist, C.; Cloots, R.; Rulmont, A.; Jerome, R.; Dubois, P. Chem Mater 2001, 13, 3830.
19. Kim, J.W.; Noh, M.H.; Choi, H.J.; Lee, D.C.; Jhon, M.S. Polymer 2000, 41, 1229.
20. Park, J.H.; Park, O.O. Korea–Australia Rheol. J 2001, 13, 13.
21. Hao, T. Adv Mater 2001, 13, 1847.
22. Kim, J.W.; Choi, H.J.; Lee, H.G.; Choi, S.B. J Ind Eng Che. 2001, 7, 218.
23. K. Kobayashi, J. Ogura, R. Kodama, T, Sakai, M. Sato, Int J Mod Phys B, 1999, 13, 1940.
24. C.W. Wu, H. Conrad, Int J Mod Phys B 1999, 13, 1713.
25. H.J. Choi, M.S. Cho, K.K. Kang, W.S. Ahn, Micropor Mesopor Mater 2000, 39, 19.
26. Ikazaki, F.; Kawai, A.; Uchida, K.; Kawakami, T.; Sakurai, K.; Anzai, H.; Asako, Y. Phys D: Appl Phys 1998, 31, 336.
27. Cho, M.S.; Choi, H.J.; Chin, I.J.; Ahn, W.S. Micropor Mesopor Mater 1999, 32, 233.
28. Böse, H. Int J Mod Phys B 1999, 13, 1878.
29. Zhao, X.P.; Yin, J.B. Chem Mater 2002, 14, 2258.
30. Quadrat, O.; Stejskal, J.; Kratochvíl, P.; Klason, C.; McQueen, D. Kubát, J.; Sáha, P. Synth Met 1998, 97, 37.
31. Lee, J.H.; Cho, M.S.; Choi, H.J.; Jhon, M.S. Colloid Polym Sci 1999, 277, 73.

32. Choi, H.J.; Kim, J.W.; To, K. Synth Met 1999, 101, 697.
33. Block, H.; Kelly, J.P.; Qin, A.; Watson, T. Langmuir 1990, 6, 6.
34. Trlica, J.; Sáha, P.; Quadrat, O.; Stejskal, J. Physica A 2000, 283, 337.
35. Lee, Y.H.; Kim, C.A.; Jang, W.H.; Choi, H.J.; Jhon, M.S. Polymer 2001, 42, 8277.
36. Kim, S.G.; Choi, H.J.; Jhon, M.S. Macromol Chem Phys 2001, 202, 521.
37. Kim, J.W.; Kim, S.G.; Choi, H.J.; Suh, M.S.; Shin, M.J.; Jhon, M.S. Int J Mod Phys B 2001, 15, 657.
38. Kim, J.W.; Liu, F.; Choi, H.J. J Ind Eng Chem. 2002, 8, 399.
39. Kim, J.W.; Choi, H.J.; Jhon, M.S. Macromol Symp 2000, 155, 229.
40. Kim, C.A.; Choi, H.J.; Kim, C.B.; Jhon, M.S. Macromol Rapid Commun 1998, 19, 419.
41. Noh, M.H.; Jang, L.W.; Lee, D.C. J Appl Polym Sci 1999, 74, 179.
42. M.; Zanetti, G.; Camino, P.; Reichert, R. Mülhaupt, Macromol Rapid Commun 2001, 22, 176.
43. Chen, G.; Liu, S.; Chen, S.; Qi, Z. Macromol. Chem Phys 2001, 202, 1189.
44. Lan, Y.; Xu, X.; Men, S.; Lu, K. Phys Rev E 1999, 60, 4336.
45. Duan, X.; Chen, H.; He, Y.; Luo, W. J Phys D: Appl Phys 2000, 33, 696.
46. Davis, L.C. J Appl Phys 1997, 81, 1985.
47. Conrad, H.; Wu, C.W.; Tang, X. Int. J. Mod Phys B 1999, 13, 1729.
48. Sohn, J.I.; Cho, M.S.; Choi, H.J.; M.S. Jhon, Macromol Chem Phys 2002, 203, 1135.
49. Sim, I.S.; Kim, J.W.; Choi, H.J.; Kim, C.A.; Jhon, M.S. Chem Mater 2001, 13, 1243.
50. Choi, H.J.; Cho, M.S.; Kim, J.W.; Kim, C.A.; Jhon, M.S. Appl Phys Lett 2001, 78, 3806.